XL CILAMCE
IBERO-LATIN AMERICAN CONGRESS ON COMPUTATIONAL METHODS IN ENGINEERING
NOVEMBER 11-14, 2019
Praiamar Natal Hotel & Convention
Natal, RN-BRAZIL

SIMULATION OF THE INTERFACIAL TRANSITION ZONE AND AIR VOIDS EFFECTS ON CONCRETE CRACKING USING A MULTISCALE FE APPROACH

Marcela Gimenes
Eduardo Alexandre Rodrigues
Osvaldo Luís Manzoli
marcela.gimenes@unesp.br
eduardo.alexandre@unesp.br
osvaldo.l.manzoli@unesp.br
São Paulo State University (UNESP)
Av. Luiz Edmundo C. Coube, 14-01, 17033-360, Bauru, SP, Brazil
Luis Antônio Guimarães Bitencourt Jr.
luis.bitencourt@usp.br
Polytechnic School at the University of São Paulo
Av. Prof. Almeida Prado, trav. do Biênio, 271, Cidade Universitária, 05508 – 900, São Paulo, Brazil

Abstract. Many models successfully consider concrete as a continuous and homogeneous material. However, mechanical and cracking behavior of concrete can be significantly dictated by its constituents and interactions between them on a finer scale. This means that considering the different phases of the mesostructure results in a more accurate modeling of concrete fracturing. Two of the concrete components that play an essential role in the mechanical response are: air voids and interfacial transition zone (ITZ), which are acknowledged as the two weakest phases of the material. Therefore, this work proposes a four-phase mesoscale representation of concrete, which consists of coarse aggregate, cement matrix, aggregate-matrix interface (ITZ) and air voids. Coarse aggregates and macro air voids are randomly embedded in the matrix. As a part of the mesh fragmentation technique (MFT) [6], high aspect ratio elements are placed between regular elements, meaning that the ITZ is explicitly represented and has its particular properties. An appropriate tension damage model is employed to describe the material nonlinear behavior. Such approach can also be extended to a multiscale approach, in which a higher refinement is given only to certain critical regions and the other regions are considered to be elastic with homogenized properties, resulting in an improved computational performance. The non-matching meshes are bonded with coupling finite elements (CFE) [8] in their shared boundaries, ensuring displacement continuity. The analysis of the ITZ and air voids effects on concrete cracking is performed by comparing the numerical responses for varied ITZ fracture properties and void ratio and size using the multiscale approach proposed. The study demonstrated that the mechanical response is extremely sensitive to the air void content, and its increase results in the formation of a very tortuous fracture and drastic drop of peak load.

Keywords: Mesoscale approach, Cracking behavior, Interfacial transition zone, Air voids.

1 Introduction

Concrete is the most usual building material and it is commonly assumed as continuous and homogeneous material for many design purposes. However, in reality, it has different constituents with different mechanical properties. Specially in reduced size specimens this heterogeneous mesostructure is more significant in such a way that cracking behavior can be dictated by the interactions between the constituents on a finer scale [1]. The size effect, related to the variation in nominal strength according to specimen size, also derives from these interactions in the micro level. Mesoscopic factors such as aggregate size and shape, interfacial transition zones (ITZs) width are proven to influence the structural response [1-4]. For example, many studies have come to the conclusion that due to their higher porosity, ITZs are the weakest regions in concrete. Thus, cracking starts and propagate more easily through them [2, 4, 5].

Besides the different constituents, concrete mesostructure is also filled with air voids. Wong et al. [6] states that in a typical concrete, the air voids volume is around 1-2% while in frost resistant concrete it is between 4% and 7%. Usually this air is entrapped because of inefficient compaction, but it might also be intentionally incorporated by means of a suitable admixture. When air voids are small and well-dispersed, they improve workability, reduce bleeding and provide freezing and thawing resistance [5, 6]. However, when the air in hardened concrete is present in the form of large voids, there is a detrimental impact, resulting in porous and poorly consolidated concrete.

Considering all the aspects mentioned above, this work proposes a four-phase mesoscale representation of concrete, which consists of coarse aggregate, cement matrix, aggregate-matrix interface (ITZ) and air voids. The reason for developing a mesoscale model is the possibility to explicitly simulate the mesostructure to study local mechanisms at the micro level such as the initiation, growth and coalescence of cracks, which affect the macroscopic concrete behavior, specially the nonlinear stage of the material. Therefore, coarse aggregates and macro air voids are randomly embedded into the matrix. As a part of the mesh fragmentation technique (MFT) [7, 8], high aspect ratio elements are placed between regular elements, meaning that the ITZ is explicitly represented and has its particular properties. An appropriate tension damage model is employed to describe the material nonlinear behavior.

Such approach can also be extended to a multiscale approach, in which a higher refinement is given only to certain critical regions and the other regions are considered to be elastic with homogenized properties, improving computational performance. The non-matching meshes are bonded with coupling finite elements (CFEs) [9] in their shared boundaries, ensuring displacement continuity.

Among the several factors that might influence concrete nonlinear behavior. In this way, this paper focuses on the ITZ and air voids effects. Their influence on concrete cracking is studied by comparing the numerical responses for varied ITZ fracture properties and void ratio and size using the multiscale approach proposed.

2 Mesh fragmentation technique

The mesh fragmentation technique proposed initially by Manzoli et al. [7] and Sánchez et al. [8] has been successfully applied to properly modeling crack propagation path. This method is based on the insertion of interface finite elements (IEs) with high aspect ratio (i.e. degenerated triangular or tetrahedral elements for 2D and 3D problems, respectively) between regular (bulk) elements of a FE mesh, as shown in Figure 1.

The main advantage of this technique is that multiple arbitrary cracks can be simulated without the need of a crack tracking scheme. In addition, the technique allows performing the analyses integrally in the context of the continuum mechanics.

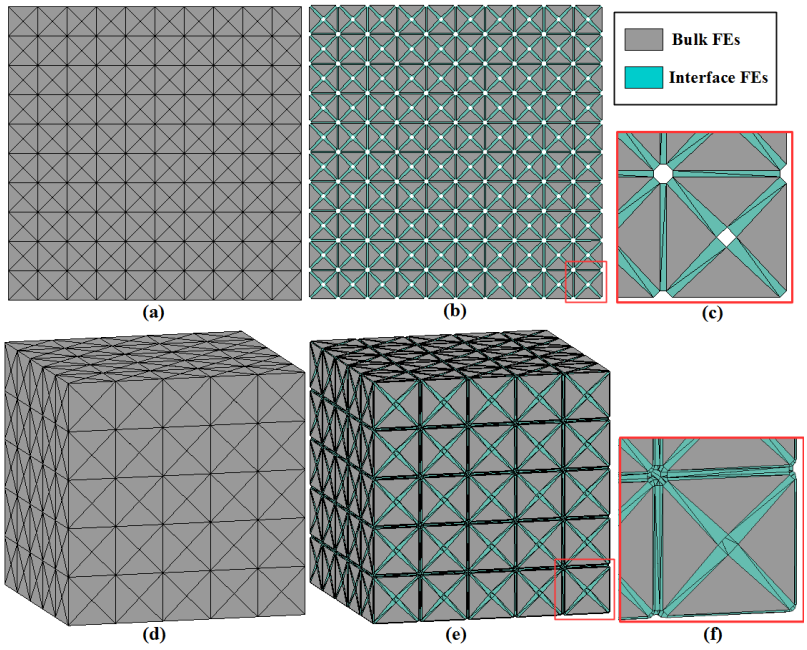

Figure 1. Mesh fragmentation technique applied for: a) 2D and b) 3D problems.

3 Constitutive damage model

The constitutive damage model employed to represent the nonlinear behavior of the standard three-node triangular interface element with high aspect ratio is incrementally formulated in the framework (context) of the implicit-explicit (IMPL-EX) integration scheme proposed by Oliver et al. [10].

In this way, for the current (actual) time step, t_{n+1}, the effective stress tensor, $\overline{\boldsymbol{\sigma}}_{n+1}$, can be calculated from the current strain tensor, ε_{n+1}, such as:

$$\overline{\boldsymbol{\sigma}}_{(n+1)} = \mathbf{C} : \boldsymbol{\varepsilon}_{(n+1)} \tag{1}$$

where $\mathbf{C}$ is the fourth order elastic tensor.

Manzoli et al. [7] demonstrated that the current strain tensor of the IE(see Figure 2) can be written as a sum of two parts, labeled as bounded and unbounded parts, showing that the strain kinematics of the IE corresponds to the typical kinematics of the continuum strong discontinuity approach (CSDA):

$$\boldsymbol{\varepsilon}_{(n+1)} = \tilde{\boldsymbol{\varepsilon}}_{(n+1)} + \hat{\boldsymbol{\varepsilon}}_{(n+1)} = \tilde{\boldsymbol{\varepsilon}}_{(n+1)} + \underbrace{\frac{1}{h}\left(\mathbf{n} \otimes [\![\mathbf{u}_{(n+1)}]\!]\right)^{s}}_{\hat{\boldsymbol{\varepsilon}}_{(n+1)}} \tag{2}$$

where $\tilde{\boldsymbol{\varepsilon}}_{(n+1)}$ and $\hat{\boldsymbol{\varepsilon}}_{(n+1)}$ are the current bounded and unbounded strain parts, respectively. The symbol $(\blacksquare)^{s}$ refers to the symmetric part of $(\blacksquare)$; h is the height of the IE (distance between the node (1) and its projection point in the element base); $\mathbf{n}$ is the unit vector normal to the element base. The symbol $\otimes$ denotes a dyadic product and $[\![\mathbf{u}_{(n+1)}]\!]$ is the current vector of the components of the relative displacement between node (1) and the point corresponding to its projection on the element base.

Since the height, h, (in Equation 2) of the element is very small ($h \to 0$), the relative displacement, $[\![\mathbf{u}_{n+1}]\!]$, corresponds to a measure of a displacement discontinuity (strong discontinuity). As previously mentioned, the strain field in Equation (2) corresponds to the typical kinematics of the CSDA, showing that the method is very attractive to represent the strain localization phenomenon that occurs during the failure process in quasi-brittle materials [10, 11].

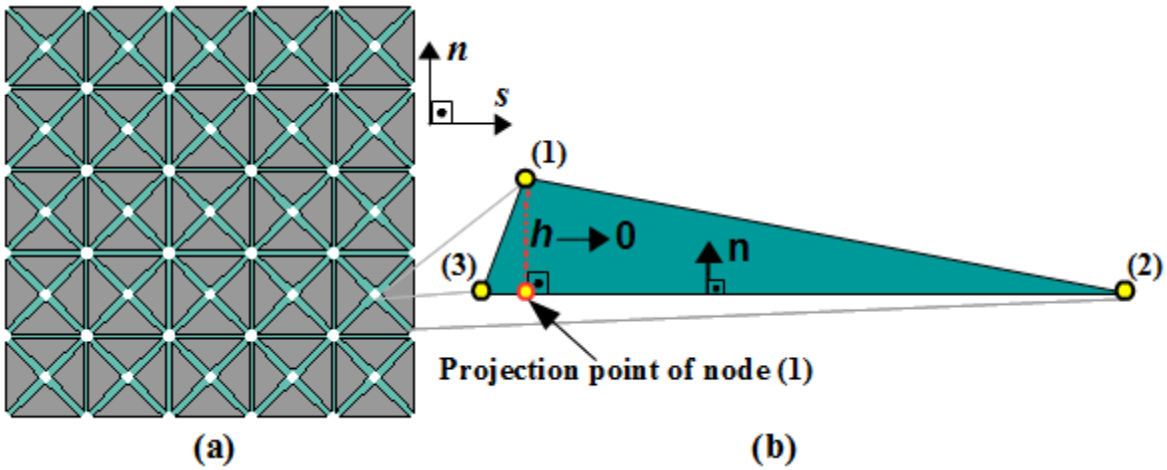

Figure 2. Solid interface element from a fragmented FE mesh.

In the field of effective stress, the damage criterion can be written as a function of the current effective stress tensor, $\bar{\boldsymbol{\sigma}}_{(n+1)}$:

$$F_{(n+1)} = \underbrace{\mathbf{n}\cdot\bar{\boldsymbol{\sigma}}_{(n+1)}\cdot\mathbf{n}}_{\sigma_{nn_{(n+1)}}} - r_{(n)} \leq 0 \tag{3}$$

where $\sigma_{nn_{(n+1)}}$ corresponds to the component of stress normal to the IE base and $r_{(n)}$ is the strain-like internal variable computed in a previous steps (i.e. in the pseudo-time steps $t_{(n)}$ and $t_{(n-1)}$.

$$\begin{cases} r_{(n)} = \sigma_{nn_{(n)}} & \text{if } F_{(n)} > 0 \\ r_{(n)} = r_{(n-1)} & \text{if } F_{(n)} \leq 0 \end{cases} \tag{4}$$

In the current step, $t_{(n+1)}$, an extrapolated strain-like internal variable can be calculated in an explicit manner, $\tilde{r}_{(n+1)}$, using those implicit one computed in the two previous steps, $t_{(n)}$ and $t_{(n-1)}$, as described below:

$$\tilde{r}_{(n+1)} = r_{(n)} + \frac{r_{(n)} - r_{(n-1)}}{\Delta t_{(n)}}\Delta t_{(n+1)}$$
$$\Delta t_{(n)} = t_{(n)} - t_{(n-1)};\quad \Delta t_{(n+1)} = t_{(n+1)} - t_{(n)} \tag{5}$$

Therefore, the current damage variable, $\tilde{d}_{(n+1)}$, is calculated in terms of the extrapolated strain-like variable, $\tilde{r}_{(n+1)}$, such as:

$$\tilde{d}_{(n+1)} = 1 - \frac{f_t}{\tilde{r}_{(n+1)}} e^{Ah\left(1-\frac{\tilde{r}_{(n+1)}}{f_t}\right)} \tag{6}$$

where f_t is the material tensile strength and h is the interface element thickness. The parameter A is softening parameter, which is related to the fractures energy, G_f, tensile strength, f_t, and Young's modulus of the material, as described in Equation (7).

$$A = \frac{f_t^2}{G_f \cdot E} \tag{7}$$

Once the damage variable is computed, it is applied to reduce all components of the effective stress tensor only if the component of stress normal to the element base, calculated in the previous step, $\sigma_{nn_{(n)}}$, is positive:

$$\tilde{\boldsymbol{\sigma}}_{(n+1)} = \begin{cases} \left(1-\tilde{d}_{(n+1)}\right)\bar{\boldsymbol{\sigma}}_{(n+1)} & if\ \bar{\sigma}_{nn(n)} > 0 \\ \bar{\boldsymbol{\sigma}}_{(n+1)} & if\ \bar{\sigma}_{nn(n)} \leq 0 \end{cases} \tag{8}$$

Finally, the corresponding algorithmic tangent operator is given by Equation (9).

$$\tilde{\mathbf{C}}^{\text{tang}}_{(n+1)} = \frac{\partial \tilde{\boldsymbol{\sigma}}_{(n+1)}}{\partial \boldsymbol{\varepsilon}_{(n+1)}} = \begin{cases} \left(1-\tilde{d}_{(n+1)}\right)\mathbf{C} & if\ \bar{\sigma}_{nn(n)} > 0 \\ \mathbf{C} & if\ \bar{\sigma}_{nn(n)} \leq 0 \end{cases} \tag{9}$$

Note that the integration scheme is developed in a closed form, i.e, from the current strain tensor, $\varepsilon_{(n+1)}$, the current stress tensor, $\tilde{\boldsymbol{\sigma}}_{(n+1)}$, is evaluated and used to fulfill the balance equation and to compute the effective algorithmic tangent operator, described in Equation (9). Furthermore, the use of IMPL-EX provides some benefits, such as: (i) the problem becomes incrementally linear and, consequently, converges in one Newton-Raphson iteration; (ii) the effective algorithmic tangent operator is symmetric and always positive definite (see Equation 9), which precludes ill-posedness and, consequently, guarantees convergence.

4 Mesoscale modeling of concrete

An explicit mesoscale modeling approach of concrete, in which this heterogeneous material is represented either by three-phase or four-phase composite material, has been proposed. In both cases, the random generation of aggregate or voids is performed using the "take-and-place" algorithm developed by Wriggers et al. [12]. The volume of particles with a given diameter interval is obtained either from the passing percentage in a grading curve or assumed from the theoretic Fuller curve [12-13].

Characterization tests provide mechanical properties of concrete as a whole (macroscopic scale), so before running the numerical analysis such properties must be particularized for each phase. Rodrigues et al. [13] and Bitencourt Jr. et al. [2] obtained the elastic phase parameters (Young's modulus and Poisson's ratio) using the mixture theory equations [12]. The fracture parameters (tensile strength and energy of fracture) were determined considering the ITZ as a 50% percentage of the matrix parameters.

4.1 Three-phase material

In this case, the mesostructure is based on a three-phase 2D and 3D representation of concrete, comprising the inclusions (coarse aggregate), mortar matrix and ITZ, as illustrated in Figure 3. The coarse aggregate are inert granular materials such as gravel or crushed stone used to give volume and reduce costs. The mortar matrix (paste phase) is a mix combination of cement, sand (fine inclusion) and water to hydrate the cement. The ITZ is a narrow region around the aggregate particle that comprises the most heterogeneous phase with high concentration of porosity. In the proposed mesoscale modeling, each of these phases is explicitly simulated and treated as a homogeneous material.

Figure 4 illustrates the general triangular and tetrahedral FE meshes adopted for 2D and 3D mesoscale discretization of concrete, respectively. These meshes are already fragmented, using the above mentioned IE with an average thickness of 100 times smaller than the bulk element. Note that due to the high ratio between the bulk and IEs, the IEs are imperceptible.

Figure 6(b) shows a highly zoomed region of the 2D mesh presented previously. In this case, it is possible to confirm that the mesh is really fragmented.

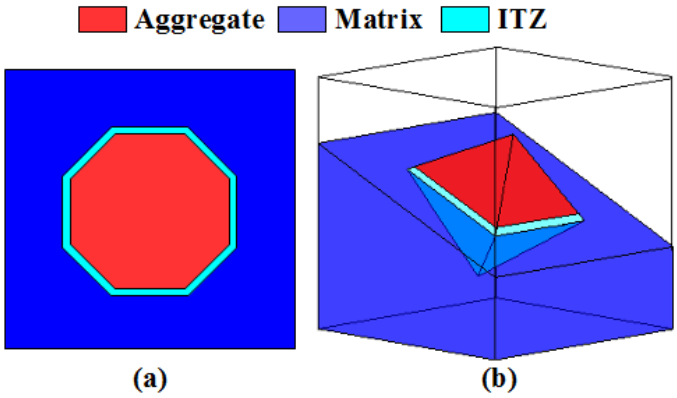

Figure 3. Three-phase composite model of concrete: (a) 2D and (b) 3D.

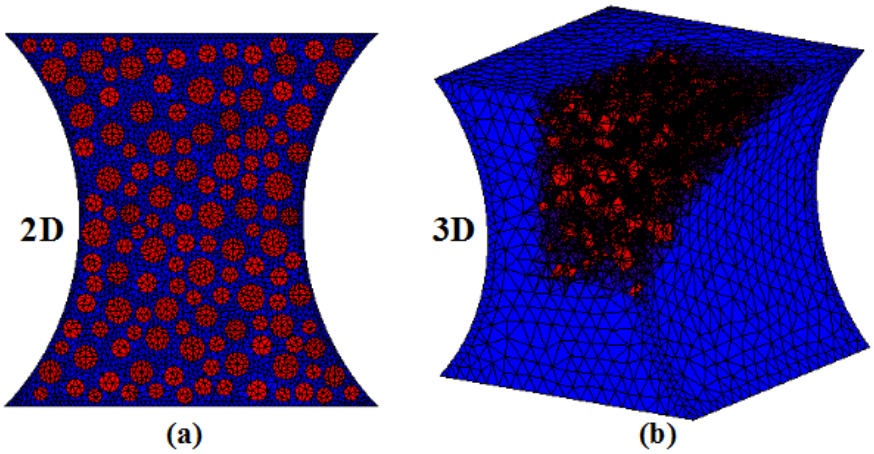

Figure 4. FE mesh for concrete in mesoscale: (a) 2D and (b) 3D.

4.2 Four-phase material

In this 2D mesoscale approach, the concrete is simulated as four-phase material including air voids, as shown in Figure 5. The take-and-place method and the simplified (octagon) geometry employed for coarse aggregates are also used for the representation of air voids. Once the generation of the coarse aggregates is finished, air voids are generated. For this purpose, the assumed input parameters are the volume fraction and the maximum and minimum air voids diameters. A linear grading curve is assumed for air voids.

Figure 6 presents the FE mesh, whose holes found in this mesh represent the macro-voids randomly distributed into the domain of the sample. In this figure, it is also possible to note the use of IE to fragment the original mesh, in order to represent potential crack paths and ITZ (Figure 6 (b)).

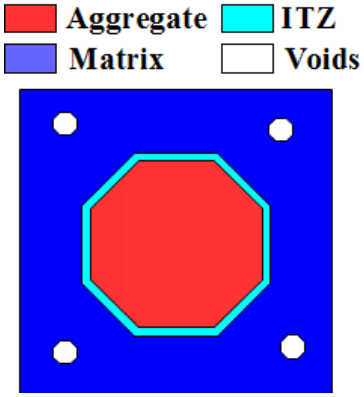

Figure 5. Four-phase composite model of concrete in 2D.

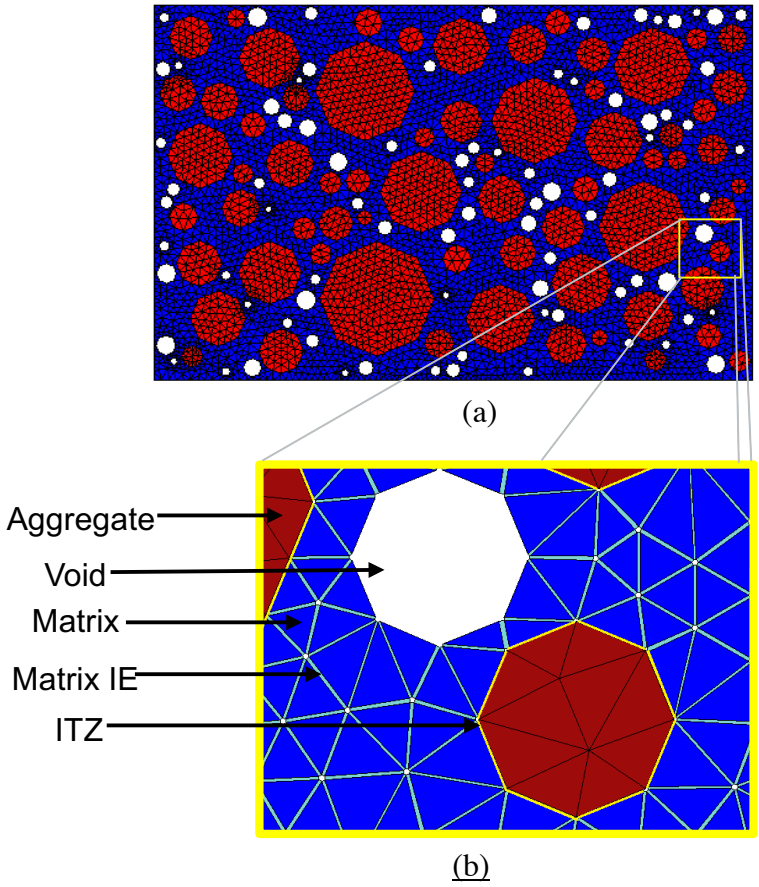

Figure 6. Four-phase material: (a) FE mesh for concrete in mesoscale and (b) detail of the different materials phase discretized in FE.

5 Concurrent multiscale modeling of concrete

The employment of a mesoscopic approach provides a better representation of the nonlinear behavior of concrete associated with damage evolution. However, it also demands more computational resources for processing as well as more preliminary steps to accurately simulate the mesostructure. Therefore, applying such approach only to the critical zones optimizes the time required for the analyses. In a concurrent multiscale approach, the areas which are more likely to suffer greater stress concentration are treated in a mesoscale, while the adjacent parts of the specimen have a macroscale approach.

5.1 Macroscale modeling of concrete

The macroscopic portion of the specimen is considered to be homogeneous and does not have to go through the mesh fragmentation process as the mesoscopic parts. Therefore, a poorer refinement is given to the macroscale, resulting in finite elements with coarse elements size.

5.2 Coupling Finite element

These two different meshes, namely macro and mesoscopic meshes are generated independently, so that their nodes not necessarily coincide. In order to provide displacement continuity, coupling finite elements (CFEs) proposed by Bitencourt Jr. et al. [9] are placed on the common boundaries of these different domains. These elements shares nodes with both meshes enforcing displacement continuity

between them. Figure 7 illustrates the CFEs applied for the multiscale modeling of concrete in two scale. Details about the CFE formulation can be found in Bitencourt Jr. et al. [9].

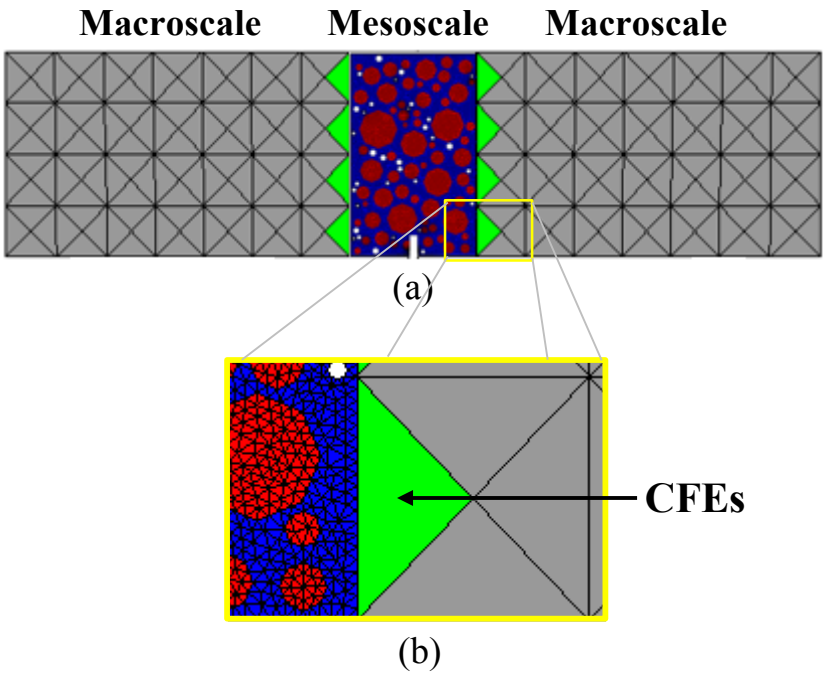

Figure 7. Details on the use of CFEs to couple the macro and mesoscopic FE meshes.

6 Numerical examples

6.1 Dog-bone test

In this example, a dog-bone specimen is tested to compare the 2D and 3D responses and also to verify parameter sensitivity regarding the ITZ strength. The specimen tested by van Vliet et al. [14] has 150mm of height, 100mm of width and 100mm of depth, as shown in Figure 8. The cross-section width is reduced to 60mm in the middle of the specimen (neck zone). It was modeled as a three-phase material where the aggregates were placed using Fuller's curve considering a volume of 35% with diameter varying from 4mm to 8mm.

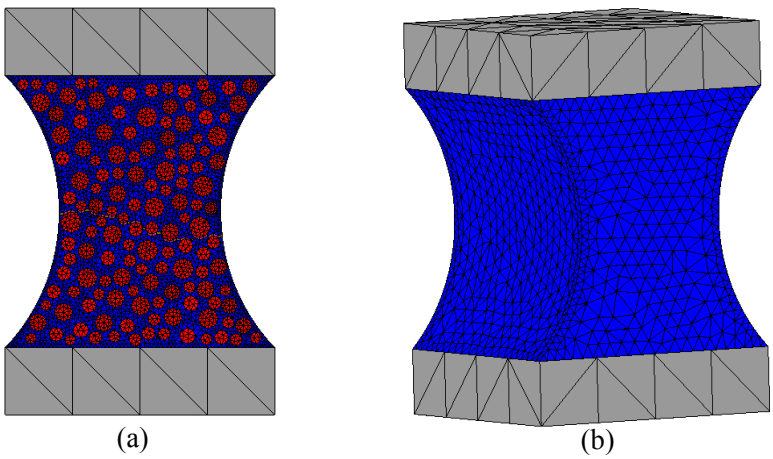

Figure 8. Dog-bone specimen in three-phase mesoscale model in (a) 2D and (b) 3D.

The specimen was submitted to uniaxial tension tests and the mean experimental value for the nominal strength of concrete was 2.97MPa. Based on that information and using the correlations

described in item 4, the parameters for each phase were determined and are displayed on Table 1. Bulk elements are considered to behave elastically, while interface elements are provided with the damage model and therefore, required fracture parameters.

Table 1: Finite elements mechanical properties.

Element	Type	E (GPa)	ν	f_t (MPa)	G_f (N/mm)
Aggregate	Bulk	50.0	0.2	-	-
Matrix	Bulk	31.5	0.2	-	-
Concrete	Bulk	38.0	0.2	-	-
Matrix - Matrix	Interface	31.5	0	4.0	0.124
ITZ	Interface	31.5	0	2.0	0.062

The 2D and 3D analyses resulted in the deformed meshes illustrated in Figure 9. As expected in accordance to the experimental, in both cases fracture propagated through the central and narrowest cross-section of the specimen featuring a very inclined fracture that grew mainly through ITZs.

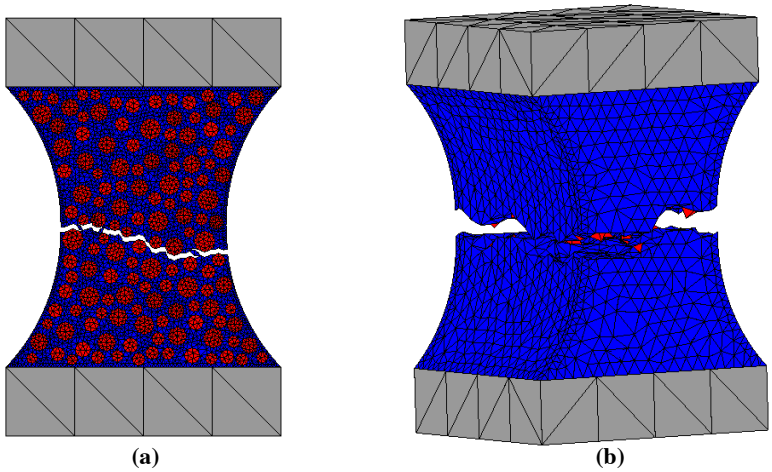

Figure 9. Fractured dog-bone specimen mesoscale model in (a) 2D and (b) 3D.

Both numerical curves (2D and 3D) are compared with the experimental one in Figure 9, where good approximation was obtained with the multiscale model. The 3D analysis was closer in terms of peak load, while the 2D analysis had a more similar residual behavior. Therefore, the 2D model was considered suitable for the succeeding examples.

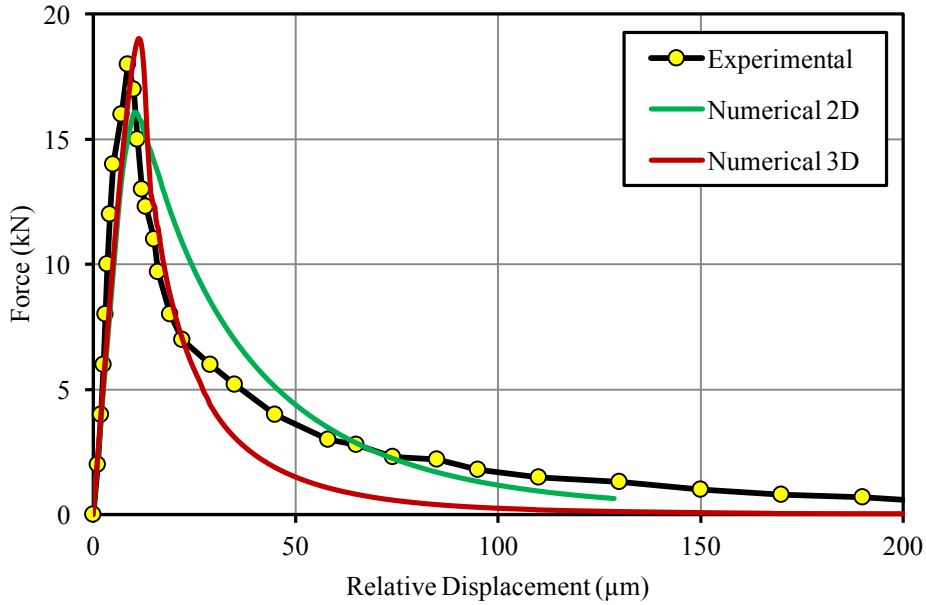

Figure 10. Load x displacement curves for the dog-bone specimen in 2D and 3D

The following analysis was performed on the same specimen but varying the ITZ strength. In the previous example, the ITZ tensile strength corresponded to 50% of the matrix tensile strength. For this analysis, such parameter assumes the values of 30%, 50%, 70% and 90% while the other parameters remain as listed in Table 1. Such configuration represents the situation of concretes made from the same paste (w/b ratio) and aggregate with same strength however with different adherence between materials.

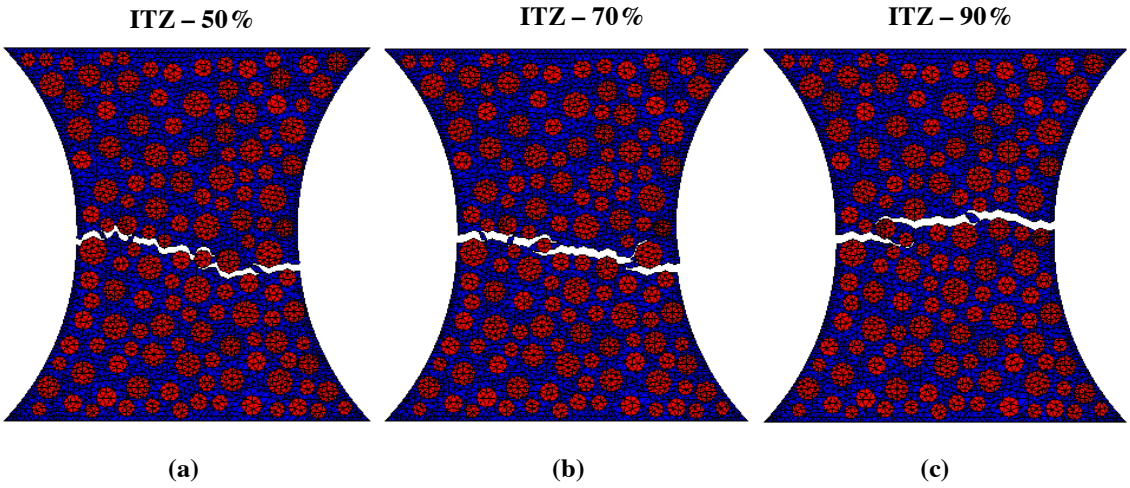

Figure 11. Fractured dog-bone specimen in three-phase mesoscale model with varied ITZ strength.

As the ITZ is the weakest phase of concrete, it is understandable the high sensitivity in the mechanical response not only in a quantitative perspective, but also in the qualitative way represent by the fractured specimens in Figure 11. As the ITZ becomes more resistant, the fracture path become less inclined, i.e., the analysis becomes similar to the homogeneous simulation of concrete, once the weakest phase contribution is minimized. Figure 12 shows the different curves obtained in this analysis, from which the high influence of the ITZ in the overall mechanical response of the specimen is verifiable. Also, comparing to the experimental curve, these results are in agreement with that 50% relation [13] between matrix and ITZ strength for typical concretes, whose ITZ is neither too porous nor too strengthened due to the use of admixtures, for example.

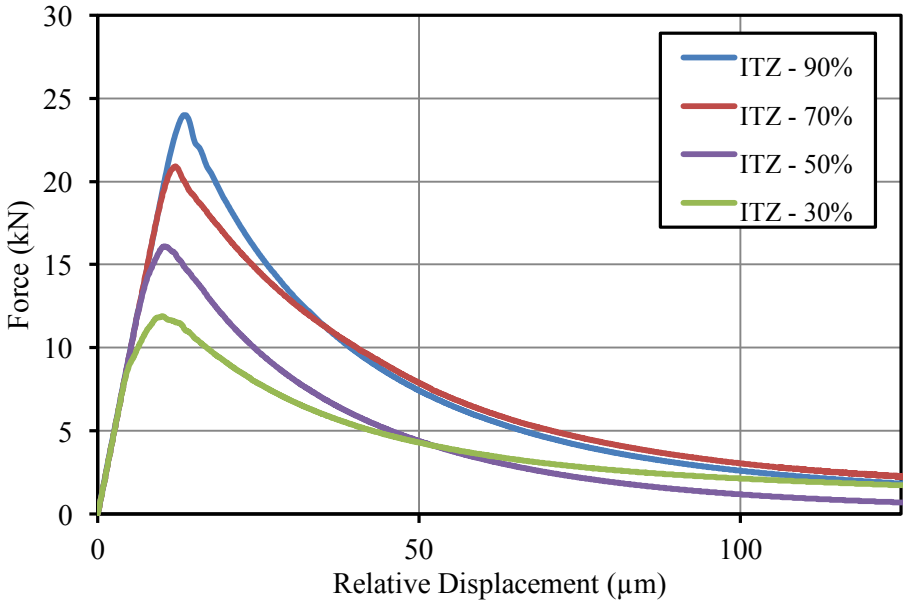

Figure 12. Load x displacement curves for the dog-bone specimen for different ITZ strengths.

6.2 Three-point bending beam

This example is based on the experiments performed by Skarzynski et al. [3] on free-supported rectangular notched concrete beams of 80mm height, 40mm depth and 32 mm length, as illustrated in Figure 13. The notch was located in the mid-span and measuring 8mm of height and 3mm of width. From the uniaxial compressive test, the following properties were obtained: compressive strength (fc) of 51.81MPa, Young's modulus (E) of 36.1GPa and Poisson's ratio (υ) equal to 0.22. Whereas from the bending test, it was obtained the tensile strength (ft) of 3.7–4.3MPa.

In order to run the numerical analysis, such homogenized properties must be properly converted into particular properties of each phase, as shown in Table 2.

Table 2: Finite elements mechanical properties.

Element	Type	E (GPa)	ν	f_t (MPa)	G_f (N/mm)
Aggregate	Bulk	47.2	0.2	-	-
Matrix	Bulk	30.6	0.2	-	-
Concrete	Bulk	36.0	0.2	-	-
Matrix - Matrix	Interface	30.6	0	3.2	0.05
ITZ	Interface	30.6	0	1.6	0.025

Once the parameters were defined, the beam discretization followed according to Figure 13. In this figure there is a visible difference between the two refinements, as there is a mesoscale (with aggregates and voids) near the notch and a macroscale near the supports.

The coupling elements are highlighted in green. The mesoscopic mesh was fragmented and the high aspect ratio elements were assigned the fracture parameters from Table 2 in order to carry nonlinearity, while the remaining elements were defined using elastic properties.

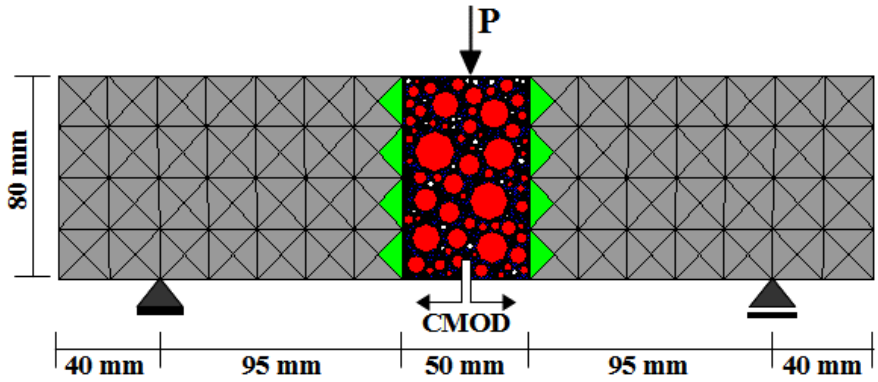

Figure 13. Multiscale modeling of notched concrete beam with four-phase material discretization.

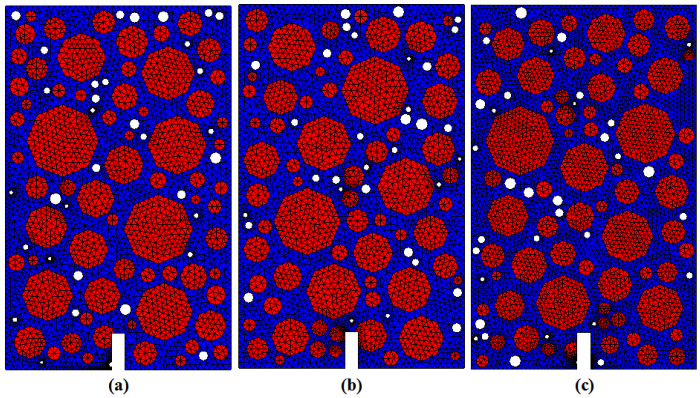

Figure 14. Different realizations of four-phase triangular FE mesh for concrete beam in mesoscale.

A four-phase material was considered where the aggregates were placed using Fuller's curve considering a volume of 35% with diameter varying from 4mm to 16mm and void size varying from 0.8 mm to 4 mm. Figure 14 shows three different realizations of the random aggregate and pore distribution in the four-phase material with a 5% volume of voids. The numerical responses were compared with the experimental ones to verify if there is distribution sensitivity.

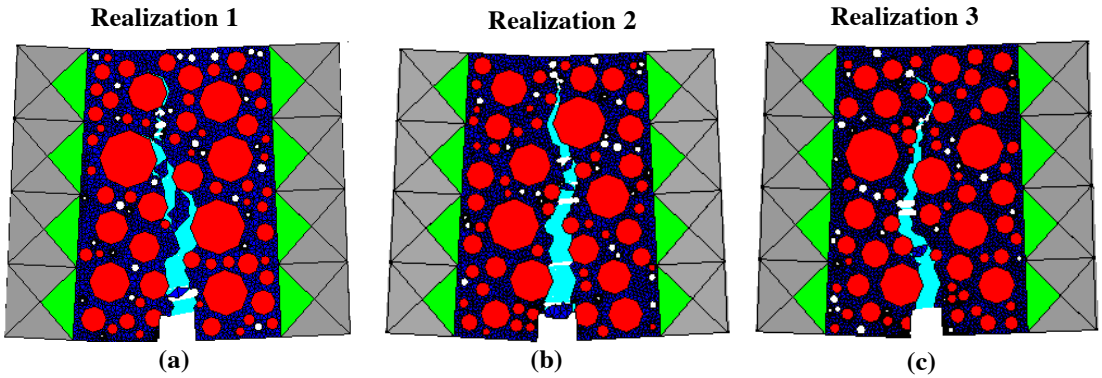

Figure 15. Fractured configuration of four-phase triangular FE mesh for concrete beam for different realizations.

Figure 15 shows the three deformed configurations, which are very similar in terms of opening displacement and inclination. This similarity can also be verified in the curves from Figure 16. The peak

load was very close for all realizations. The fracture energy was also very close for realizations 2 and 3 while realization 1 has dissipated slightly more energy. Also, the curves are very close to the experimental curve obtained by Skarzynski et al. [3].

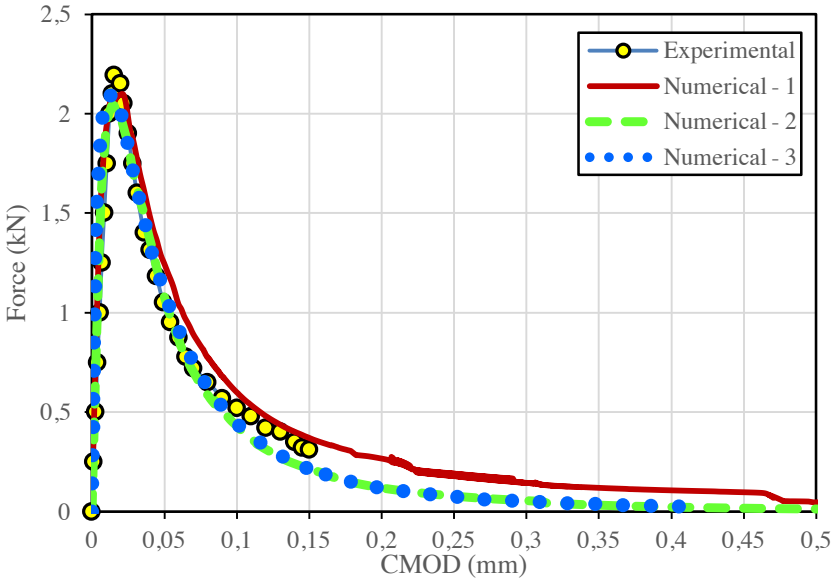

Figure 16. Load x CMOD curves for concrete beam with 5% volume of air voids.

Finally, the same beam was tested for the hypothesis of higher volumes of voids that could result from the conditions described in the introductory section of this work. The responses for 5%, 8% and 12% of voids are shown in Figures 17. As the amount of voids increases, the fracture becomes more tortuous and with larger opening. From the curves in Figure 18, it is possible to observe that the increase of voids causes a drastic drop in the peak load but has little effect on the residual response.

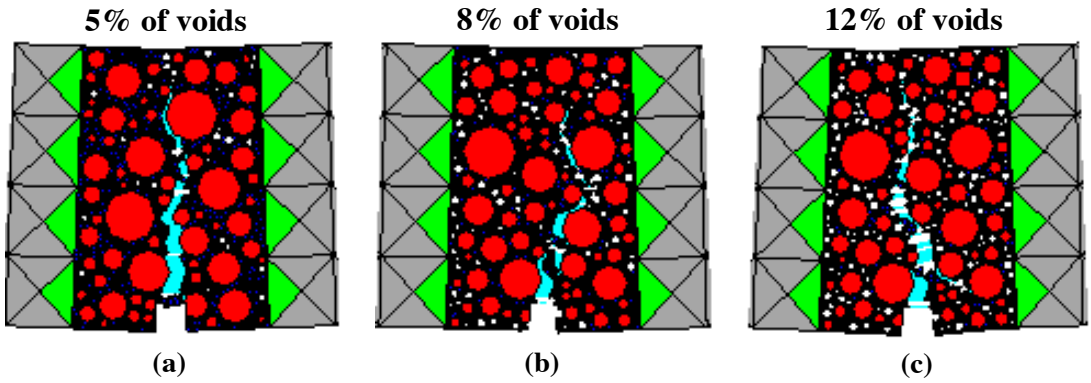

Figure 17. Deformed four-phase triangular FE meshes for a concrete beam in mesoscale with different volumes of air voids.

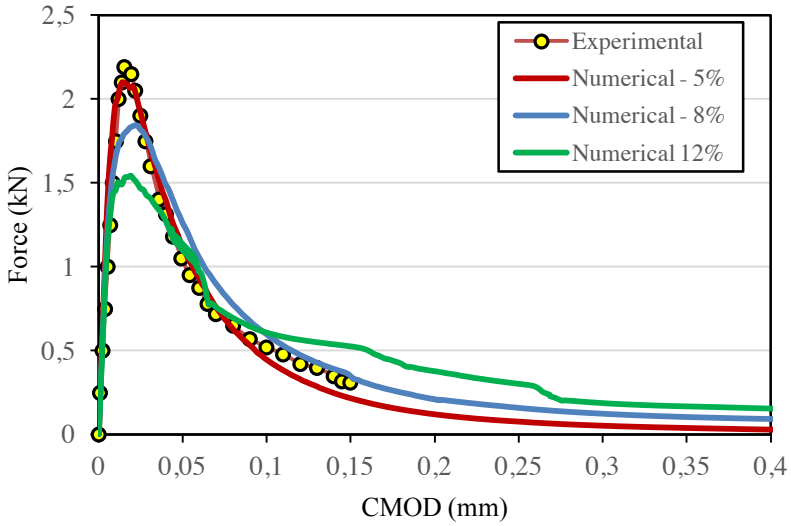

Figure 18. Load x CMOD curves for concrete beam with 5%, 8% and 12% of air voids.

7 Conclusions

This paper studied the influence of the ITZs and voids in the mechanical behavior of concrete using a concurrent two-scale model based on the application of a mesh fragmentation technique. First, a sensibility analysis of a dog-bone specimen was performed comparing 2D and 3D models. The responses were slightly different, but the 2D analysis was close enough to the experimental response. Also, it was observed that the relation of 50% between the ITZ and matrix tensile strength was more adequate to simulate the mechanical behavior of typical concrete. The numerical response was very sensitive to the ITZ strength both qualitatively and quantitatively. The attribution of very high strength to the ITZ causes the analysis becomes similar to the simulation of homogeneous concrete.

The 2D concurrent model was applied to simulate the experiment conducted by Skazynski et al. [3] in notched beams with determined air void content. Different realizations were performed in order to attest the absence of distribution bias. Once the numerical curves were close to the experimental ones, the work proceeded to the study of void influence. Such study demonstrated that the mechanical response is extremely sensitive to the air void content, and its increase results in the formation of a very tortuous fracture and drastic drop of peak load.

Acknowledgements

The authors wish to acknowledge the financial support of the São Paulo Research Foundation (FAPESP – Proc.: 2018/05784-3), National Council for Scientic and Technological Development (CNPq – Proc.: 423379/2016-0), and Coordination for the Improvement of Higher Education Personnel (CAPES).

References

[1] Y. Huang , Z. Yang, W. Ren, G. Liu, C. Zhang. “3D meso-scale fracture modelling and validation of concrete based on in-situ X-ray Computed Tomography images using damage plasticity model”, International Journal of Solids and Structures V. 67–68, pp. 340-352, 2015.

[2] L.A.G. Bitencourt Jr., M. Gimenes, E.A. Rodrigues, O.L. Manzoli. “A concurrent two-scale

approach for high strength concrete". *Proceedings of the 10th International Conference on Fracture Mechanics of Concrete and Concrete Structures*, 2019.

[3] L. Skarzynski, M. Nitka, J. Tejcheman. "Modelling of concrete fracture at aggregate level using FEM and DEM based on X-ray μCT images of internal structure". *Engineering Fracture Mechanics,* Vol. 147, pp. 13-35, 2015.

[4] H.K. Man, J.G.M. van Mier. "Size effect on strength and fracture energy for numerical concrete with realistic aggregate shapes". *Int. Journal of Fracture*, Vol. 174, pp. 61-72, 2008.

[5] X. Wang, Z. Yang, A. Jivkov. "Monte Carlo simulations of mesoscale fracture of concrete with random aggregates and pores: a size effect study*". Construction and Building Materials*, Vol.80, pp. 262-272, 2015.

[6] H.S. Wong, A.M. Pappas, R.W. Zimmerman, R.N. Buenfeld. "Effect of entrained air voids on the microstructure and mass transport properties of concrete". *Cement and Concrete Research,* Vol. 41, pp. 1067-1077, 2011.

[7] O.L. Manzoli, M.A. Maedo, L.A.G. Bitencourt Jr., E.A. Rodrigues, "On the use of finite elements with a high aspect ratio for modeling cracks in quasi-brittle materials", *Engineering Fracture Mechanics*, Vol. 153, pp. 151-170, 2016.

[8] M. Sánchez, O.L. Manzoli, L.J.N. Guimarães. "Modelling 3-D desiccation soil crack networks using a mesh fragmentation technique". *Computers and Geotechnics* Vol. 62, pp. 27-39, 2014.

[9] L.A.G. Bitencourt Jr., O.L. Manzoli, P.G.C. Prazeres, E.A. Rodrigues, T.N. Bittencourt, "A coupling technique for non-matching finite element meshes", *Computer Methods in Applied Mechanics and Engineering*, Vol. 290, 19-44, 2015.

[10] J. Oliver, A. Huespe, *P. Sánchez.* "A comparative study on finite elements for capturing strong discontinuities: E-FEM vs X-FEM". *Comput Methods Appl Mech Engng*, Vol. 195, pp. 4732-475. 2006.

[11] J. Oliver, A. Huespe, O.L. Manzoli. "Strong discontinuities and continuum plasticity models: the strong discontinuity approach". *International Journal of Plasticity* 15, pp. 319- 351. 1999.

[12] P. Wriggers, S.O. Moftah. "Mesoscale models for concrete: homogenization and damage behaviour". *Finite Elements in Analysis and Design*, Vol. 42, pp. 623–636. 2006.

[13] E.A. Rodrigues, O.L. Manzoli, L.A.G. Bitencourt Jr., T.N. Bittencourt. "2D mesoscale model for concrete based on the use of interface element with a high aspect ratio". *International Journal of Solids and Structures, Vol. 94-95*; pp. 112-124, 2006.

[14] M.R.A. van Vliet, J.G.M. van Mier. "Experimental investigation of size effect in concrete and sandstone under uniaxial tension". *Engineering Fracture Mechanics 65* (2000) pp.165-188.